Structures of Phage-Display Peptides that Bind to the Malarial Surface Protein, Apical Membrane Antigen 1, and Block Erythrocyte Invasion†

David W. Keizer,‡ Luke A. Miles,‡,§ Felomena Li,||,⊥ Margie Nair,§ Robin F. Anders,||,@ Andrew M. Coley,||,⊥,@ Michael Foley,*,||,⊥,@ and Raymond S. Norton*,‡,§

The Walter & Eliza Hall Institute of Medical Research, 1G Royal Parade, Parkville, Victoria 3050, Australia, Biomolecular Research Institute, 343 Royal Parade, Parkville 3052, Australia, and Department of Biochemistry, Cooperative Research Centre for Diagnostics, and Cooperative Research Centre for Vaccine Technology, La Trobe University, Bundoora, Victoria 3083, Australia

Received March 7, 2003; Revised Manuscript Received May 21, 2003

ABSTRACT: Apical membrane antigen 1 (AMA1) of the human malaria parasite *Plasmodium falciparum* is synthesized by schizont stage parasites and has been implicated in merozoite invasion of host erythrocytes. Phage-display techniques have recently been used to identify two 15-residue peptides, F1 and F2, which bind specifically to *P. falciparum* AMA1 and inhibit parasite invasion of erythrocytes [Li, F., *et al.* (2002) *J. Biol. Chem. 277*, 50303−50310]. We have synthesized F1, F2, and three peptides with high levels of sequence identity, determined their relative binding affinities for *P. falciparum* AMA1 with a competition ELISA, and investigated their solution structures by NMR spectroscopy. The strongest binding peptide, F1, contains a β-turn that includes residues identified via an alanine scan as being critical for binding to AMA1 and inhibition of merozoite invasion of erythrocytes. The three F1 analogues include a 10-residue analogue of F1 truncated at the C-terminus (tF1), a partially scrambled 15-mer (sF1), and a disulfide-constrained 14-mer (F1tbp) which is related to F1 but has a sequence identical to that of a disulfide-constrained loop in the first epidermal growth factor module of the latent transforming growth factor-β binding protein. tF1 and F1tbp bound competitively with F1 to AMA1, and all three contain a type I β-turn encompassing key residues involved in F1 binding. In contrast, sF1 lacked this structural motif, and did not compete for binding to AMA1 with F1; rather, sF1 contained a type III β-turn involving a different part of the sequence. Although F2 was able to bind to AMA1, it was unstructured in solution, consistent with its weak invasion inhibitory effects. Thus, the secondary structure elements observed for these peptides in solution correlate well with their potency in binding to AMA1 and inhibiting merozoite invasion. The structures provide a valuable starting point for the development of peptidomimetics as antimalarial antagonists directed at AMA1.

Apical membrane antigen 1 (AMA1) is a surface-exposed, type 1 integral membrane protein conserved throughout all *Plasmodium* species. It is critical for the invasion of host red blood cells (RBCs) (*2*), and is translocated from the rhoptries to the apical end of the merozoite surface near the time of invasion (*3*−*5*), although its precise role in this process remains undefined. It has been postulated that AMA1 is involved in realignment of the parasite following attachment to the RBC, ensuring that the apical prominence of the merozoite is in the proximity of the RBC surface (*6*). AMA1, which appears to be a target of naturally acquired protective antibody responses, is a leading candidate for inclusion in a malaria vaccine and a target for the development of antimalarial therapeutics. Recombinant AMA1 induced protective immune responses in mouse and monkey models against *Plasmodium chabaudi adami* and *Plasmodium fragile*, respectively (*7*−*10*), and both monoclonal and polyclonal antibodies against AMA1 inhibit merozoite invasion of RBC (*9*−*14*). The observation that it was not possible to obtain targeted gene disruptions of the AMA1 gene that knocked out the function of the protein further supports an important role for AMA1 in the invasion of host erythrocytes (*15*). An orthologue of AMA1 found in the related apicomplexan parasite *Toxoplasma gondii* presumably plays a role in the invasion of cell types other than erythrocytes by this pathogen (*16*, *17*).

Phage-display techniques have been used in a range of applications to identify peptides that can bind to organ-specific molecules (*18*, *19*), recognize DNA (*20*), and mimic carbohydrate structures (*21*) and clinically important antibodies (*22*). The structures of several of these peptides, both in solution and bound to their receptors, have been determined

† This work was supported in part by grants from the Australian National Health and Medical Research Council and the UNDP/World Bank/WHO Special Programme for Research and Training in Tropical Diseases (TDR).

* To whom correspondence should be addressed: The Walter & Eliza Hall Institute of Medical Research, NMR Laboratory, 381 Royal Parade, Parkville, Victoria 3052, Australia. Phone: +61 3 9903 9650. Fax: +61 3 9903 9655. E-mail: Ray.Norton@wehi.edu.au.

‡ The Walter & Eliza Hall Institute of Medical Research.

§ Biomolecular Research Institute.

|| Department of Biochemistry, La Trobe University.

⊥ Cooperative Research Centre for Diagnostics, La Trobe University.

@ Cooperative Research Centre for Vaccine Technology, La Trobe University.

10.1021/bi034376b CCC: $25.00
Published on Web 07/30/2003

F1	G W **R** L *L* **G F G P** A S S **F S** M
tF1	G W **R** L *L* **G F G P** A
sF1	A M S P W F **R** S *L* **G F G** S L G
F1tbp	C K *I* **G F G P** D P T **F S** S C
F2	T R L F **R** V **P V** L P S G **V** T S
F3	P F A **R** A **P V** E H H D **V** V G L

FIGURE 1: Sequences of peptides that interact with AMA1. Peptides F1−F3 were previously identified from a phage-display library (*1*). The peptide tF1 is a truncated version of the F1 peptide that was designed on the basis of the alanine scan of F1 to identify critical residues. sF1 represents an inactive version of F1 containing the same amino acid residues but in a different sequence. F1tbp is a constrained version of F1 by virtue of incorporation of a disulfide bond. Peptides F1, tF1, sF1, and F1tbp are aligned to show the conserved core; identical and conserved residues are shown in bold and italics, respectively. F2 and F3 are aligned according to the consensus sequence defined by Li *et al.* (*1*).

using nuclear magnetic resonance (NMR) and X-ray crystallography (*23*−*25*). In recent work by Li *et al*. (*1*), a library of random 15-residue peptides expressed as part of the minor coat protein gpIII of filamentous phage were panned on immobilized AMA1. Phage with the highest binding affinity for AMA1 were selected for DNA sequencing. These data yielded three different peptide sequences denoted F1−F3 (Figure 1), which were subsequently characterized on the basis of their ability to bind specifically to recombinant and native AMA1, and their ability to block merozoite invasion of RBC.

The first peptide, F1, represented the majority of clones isolated from the phage-display library. This peptide, which had the highest affinity for *Plasmodium falciparum* AMA1 but was unable to bind to *P. chabaudi* AMA1, was the most effective peptide at inhibiting merozoite invasion of RBC. An alanine scan of F1 indicated that the pentapeptide sequence $Leu^5Gly^6Phe^7Gly^8Pro^9$ was critical for both binding to AMA1 and invasion inhibition (*1*). On the basis of this result, a 10-residue truncated version of F1 (tF1), which lacked the five C-terminal residues of F1, was synthesized and shown to have the same biological activity as F1. The final peptide in this series, F1tbp, is related to F1 and was synthesized after a BLAST search revealed that the sequence of F1 was homologous with that of the first epidermal growth factor (EGF) module of the latent transforming growth factor-β binding protein, particularly in the region of the key pentapeptide sequence. This sequence was contained in a disulfide-constrained loop in this protein, and so a peptide incorporating this sequence, including the disulfide, was produced and shown not only to bind to AMA1 but also to compete with the binding of F1. The solution structure of this peptide has been determined and compared with the corresponding region of known EGF structures.

Peptides F2 and F3 contain the consensus motif XXRXPVXXXXV, where the first two residues are hydrophobic. Although both peptides had lower relative binding affinities for *P. falciparum* AMA1 than F1, they were able to compete for AMA1 in the presence of phage displaying F1 and were also able to inhibit merozoite invasion, albeit at concentrations 10-fold higher than that required for F1. In contrast to F1, both F2 and F3 were able to bind to both *P. falciparum* AMA1 and *P. chabaudi* AMA1. This suggests that the binding epitopes for each of the three peptides, F1−F3, overlap at least partially, but are not identical. Each of these peptides had no effect on parasite development when added after merozoites had successfully entered the RBC. In this study, we have investigated the solution structures of four peptides in these two families and report on the biological properties and structures of several analogues based on the most active peptide, F1.

MATERIALS AND METHODS

Peptides. All synthetic peptides investigated in competition ELISAs and by NMR spectroscopy were prepared by AUSPEP Pty Ltd. (Parkville, Victoria, Australia). The correct mass of each peptide was verified by mass spectrometry, and the overall purity (>90%) was confirmed by reverse phase HPLC. The sequences of these peptides are shown in Figure 1.

Competition ELISAs. A competitive binding assay based on ELISA techniques was used to determine whether any of the synthetic peptides were able to block the binding of F1 phage to *P. falciparum* AMA1. Plates (96 wells) were coated with 0.5 μg of *P. falciparum* AMA1 in 100 μL of 0.1 M Na_2HCO_3 (pH 8.5) per well at 4 °C overnight. Wells were then blocked with 300 μL of 0.5% (w/v) BSA in PBS for 2 h at room temperature followed by three washes with PBS. Then 10^{10} phage particles and 10 μg of the appropriate peptide in 100 μL of 0.5% (w/v) PBS were added to each well (corresponding to 65 μM for each of the peptides except tF1, which was at 95 μM) and incubated at room temperature for 1 h. Wells were then washed with PBS-T (0.5% Tween 20) five times. Bound phage particles were detected using a 1:3000 dilution of an anti-M13-HRP antibody (Amersham Pharmacia Biotech, Castle Hill, New South Wales, Australia) in PBS with *o*-phenylenediamine as the enzyme substrate. Each set of conditions was repeated in duplicate.

Peptide Inhibition of Merozoite Invasion of RBCs. P. falciparum cloned lines 3D7 and HB3 were cultured continuously as described by Trager and Jensen (*26*). For invasion assays, *P. falciparum* cloned lines were grown to parasitaemias of approximately 10% and erythrocytes infected with mature-stage (schizont) parasites were purified on a Percoll cushion (*27*). The infected erythrocytes were adjusted to 3−4% parasitaemia and 2% haematocrit and aliquoted into wells containing 50 μmol of F1, tF1, or sF1 or no peptide. Approximately 20 h later, smears were made to determine the number of invaded cells, identified as those cells containing rings. Parasitaemia levels were determined by counting 1000 cells from Giemsa-stained thin blood films. Each set of conditions was repeated in duplicate.

NMR Spectroscopy. Samples were prepared for NMR by dissolving lyophilized peptides in a 10% ^2H_2O/90% H_2O mixture to a final concentration of approximately 2.5 mM. The pH was adjusted to 4.5, but no buffer was present. Two-dimensional homonuclear TOCSY spectra with a mixing time of 37.5 ms and E-COSY NMR spectra were collected on a Bruker AMX-500 spectrometer. NOESY spectra with a mixing time of 250 ms were collected on a Bruker DRX-600 spectrometer. $^1H-^{13}C$ HMQC spectra for the assignment of ^{13}C chemical shifts (*28*, *29*) were collected using 2.5 mM samples of natural-abundance F1 and tF1 in 100% ^2H_2O on a Bruker AMX-500 spectrometer. Diffusion measurements were performed using a PFG longitudinal eddy-current delay pulse sequence (*30*, *31*) as implemented by Yao *et al*. (*32*).

Table 1: Summary of Experimental Constraints and Structural Statistics for Peptides F1, tF1, sF1, and F1tbp

	F1	tF1	sF1	F1tbp
no. of distance restraints	93	83	70	91
intraresidue ($i = j$)	51	38	21	29
sequential ($\|i - j\| = 1$)	29	37	34	51
medium-range ($1 < \|i - j\| < 5$)	13	6	15	21
no. of dihedral restraints	10	5	2	8
energies[a]				
E_{NOE} (kcal mol^{-1})	12.3 ± 1.9	6.0 ± 1.4	5.4 ± 1.4	11.0 ± 2.0
deviations from ideal[b]				
bonds (Å)	0.0090 ± 0.0006	0.0049 ± 0.0005	0.0042 ± 0.0003	0.0069 ± 0.0001
angles (deg)	1.01 ± 0.09	0.57 ± 0.05	0.47 ± 0.03	0.73 ± 0.07
impropers (deg)	0.76 ± 0.06	0.43 ± 0.06	0.34 ± 0.04	0.30 ± 0.05
rms deviations[c]				
backbone atoms (global)	>2	1.74	>2	0.98
backbone atoms [$S(\phi)$ and $S(\psi) > 0.8$]	0.26	0.42	0.23	0.47
Ramachandran plot[d] (%)				
most favored	64.5	79.0	64.0	61.8
allowed	35.5	21.0	28.5	38.2
additionally allowed	0	0	1.5	0
disallowed	0	0	6.0[e]	0

[a] The values for E_{NOE} are calculated from a square-well potential with force constants of 50 kcal mol^{-1} Å^2 after minimization in a water box as described in Materials and Methods. Values prior to water minimization were 0.12 ± 0.01, 0.65 ± 0.03, 0.06 ± 0.02, and 3.6 ± 0.05 kcal mol^{-1} for F1, tF1, sF1, and F1tbp, respectively. The rmsd values over the backbone heavy atoms (N, C$^\alpha$, and C) were compared before and after water minimization over the well-ordered residues ($S_{\phi,\psi} > 0.8$); for each peptide, the rmsd was less than 0.5 Å. [b] The values for the bonds, angles, and impropers show the deviations from ideal values based on perfect stereochemistry. [c] The rmsd over the backbone heavy atoms (N, C$^\alpha$, and C) over the indicated residues. [d] As determined by the program PROCHECK-NMR for all residues except Gly and Pro (*39*). [e] Residues in the disallowed region for sF1 were all located in the unstructured C-terminal tail.

All spectra were collected at 5 °C unless otherwise stated and were referenced to an impurity peak present at 0.15 ppm. Spectra were processed using XWINNMR (version 1.3, Bruker Biospin) and analyzed using XEASY (version 1.3.13) (*33*). Tables of chemical shift assignments for peptides F1, tF1, F1tbp, and sF1 have been deposited in the BioMagResBank (*34*) as entries 5476, 5477, 5478, and 5479, respectively.

Structure Calculations. Structures for the major conformation of each peptide investigated in this study were calculated using distance restraints from two-dimensional NOESY spectra acquired at 600 MHz. A series of amide exchange experiments on the F1 peptide (pH 4.5 and 5 °C) failed to show any slowly exchanging amides, and no amide temperature coefficients ($\Delta\delta/\Delta T$) with a magnitude of <5.6 ppb/K were observed in F1, tF1, or sF1. Temperature coefficient magnitudes ($|\Delta\delta/\Delta T|$) of >4−5 ppb/K generally indicate an exposed amide proton, whereas values of <3 ppb/K indicate an amide proton that is shielded from solvent (*35*). As a result of these two experiments, no hydrogen bond restraints were included in any structural calculations. Changes in amide proton chemical shifts were linear over the temperature range examined (5−35 °C), indicating no significant fluctuations in conformation over this range.

Dihedral restraints for ϕ angles are summarized in Table 1. $^3J_{HNH\alpha}$ values were measured from a DQF-COSY spectrum and converted to ϕ dihedral restraints as follows: $^3J_{HNH\alpha} > 8$ Hz, $\phi = -120 \pm 30°$; $^3J_{HNH\alpha} < 6$ Hz, $\phi = -60 \pm 30°$. Where positive ϕ angles could be excluded on the basis of NOE data, ϕ angles were restricted to a negative value ($\phi = -90 \pm 90°$). For each peptide, cis−trans isomerization of a proline residue was observed, identified by the presence of characteristic NOEs and the presence of peak splitting for the prolines and preceding residues. The percentage of the cis conformation was estimated to be no more than 5% for each peptide, and in each case, families of structures were calculated only for the dominant trans conformation.

Intensities of NOE cross-peaks assigned in XEASY were calibrated using the CALIBA macro from the program DYANA (version 1.5) (*36*). NOEs providing no restraint or representing fixed distances were removed. Initial structures were then calculated using torsion angle dynamics and simulated annealing protocols in DYANA with the experimental restraints. These structures were optimized for a low target function which comprises terms for NOE and dihedral angle violations. The final constraint set was then used to calculate a new family of 200 structures using the standard simulated annealing script supplied with CNS (version 1.1) (*37*). Distance geometry routines were not used as the flexible regions of these peptides were found not to sample the full conformational space allowed by the restraints, resulting in regions of apparently well-ordered backbone. The 50 lowest-energy structures were selected, and a box of water was built around the peptide structure using the OPLSX parameter set described by Linge and Nilges (*38*). This was then energy minimized on the basis of NOE and dihedral restraints and the geometry of the bonds, angles, and impropers. From this set of structures, a final family of 20 lowest-energy structures was chosen for analysis using PROCHECK-NMR (*39*) and MOLMOL (*40*). The final structures had no experimental distance violations greater than 0.2 Å or dihedral angle violations greater than 5°. All structural figures were prepared using the program MOLMOL (*40*).

RESULTS

Peptides. NMR spectroscopy has been used to determine the structures of peptides identified by phage display as binding to *P. falciparum* AMA1. F1 was investigated as it was the most represented sequence in the final family of peptides selected by phage display, had the highest relative binding affinity for *P. falciparum* AMA1, and was the most effective peptide at inhibiting merozoite invasion. F2 was included because it represented a different sequence motif that was able to bind both *P. falciparum* and *P. chabaudi*

AMA1 (unlike F1) and was able to inhibit merozoite invasion. The other three peptides that were investigated were related to F1. A 10-residue version of F1 truncated at the C-terminus was designed that retained the biological properties of F1. sF1 is a related peptide with the same amino acid composition as F1 but a partially scrambled sequence (Figure 1). The sF1 peptide was used as a negative control because of its complete lack of binding and biological activity (see below).

A BLAST search (*41*) with the F1 sequence identified a related sequence within a loop region of the human latent transforming growth factor-β binding protein (*42*, *43*) that was naturally constrained by a disulfide bridge. This sequence shares a consensus motif with F1 and tF1 consisting of a hydrophobic residue (L/I) followed by GFGP (Figure 1). A peptide corresponding to this disulfide-constrained loop, F1tbp, was therefore synthesized for analysis in this study.

Peptide Binding to P. falciparum AMA1. Each peptide was examined by the ELISA for its ability to compete with phage displaying F1 for binding to *P. falciparum* AMA1. Initially, 10^{10} phage particles per mL were incubated with immobilized *P. falciparum* AMA1 in the presence or absence of 10 μg of each of the peptides, F1−F3 (Figure 2A). This showed that the F1 peptide competed effectively with the phage particles displaying the same peptide for binding to *P. falciparum* AMA1, reducing the level of binding of phage by 87%. In contrast, the control peptide sF1 was unable to compete. Despite their lack of sequence homology, peptides F2 and F3 competed with the phage particles, albeit to a lesser extent than F1 (reducing the level of phage binding by 53 and 33%, respectively). In a second series of competition assays using increasing amounts of peptide, each member of the F1 peptide family was examined for its ability to compete with phage displaying F1 (Figure 2B). Consistent with previous observations, F1 was the most efficient competitor at all concentrations, while sF1 was not able to compete for binding at concentrations up to 300 μM. Both tF1 and F1tbp could compete with the phage at all concentrations tested with only slightly reduced affinities relative to F1. In a separate series of assays, each of the peptides (F1, tF1, sF1, and F1tbp) was immobilized in the wells of a microtiter plate and their ability to capture free *P. falciparum* AMA1 assayed by detection with rabbit *P. falciparum* AMA1 antiserum followed by HRP-conjugated anti-rabbit IgG antibody (Figure 2C). F1 was the most efficient at capturing *P. falciparum* AMA1, closely followed by both tF1 and F1tbp, whose activities were indistinguishable from each other. By comparison, the sF1 peptide had little ability to capture *P. falciparum* AMA1.

Merozoite Invasion of Red Blood Cells. AMA1 is believed to play an essential role in the invasion of RBC by the malarial parasite (*9*, *11*, *14*). As binding of F1 and tF1 to *P. falciparum* AMA1 was observed *in vitro*, an invasion inhibition assay was performed to determine whether these peptides could inhibit parasite invasion of RBCs. Parasites from cloned strains 3D7 and HB3 were incubated with RBCs in the presence or absence of F1, tF1, and sF1 (Figure S1). F1 and its truncated form inhibited the invasion of RBCs by 3D7 merozoites by approximately 60%, with an IC_{50} of 10 μM, whereas sF1 was not inhibitory. This result agrees well with the alanine scan of Li *et al.* (*1*), which showed that none of the residues critical for the *P. falciparum* AMA1

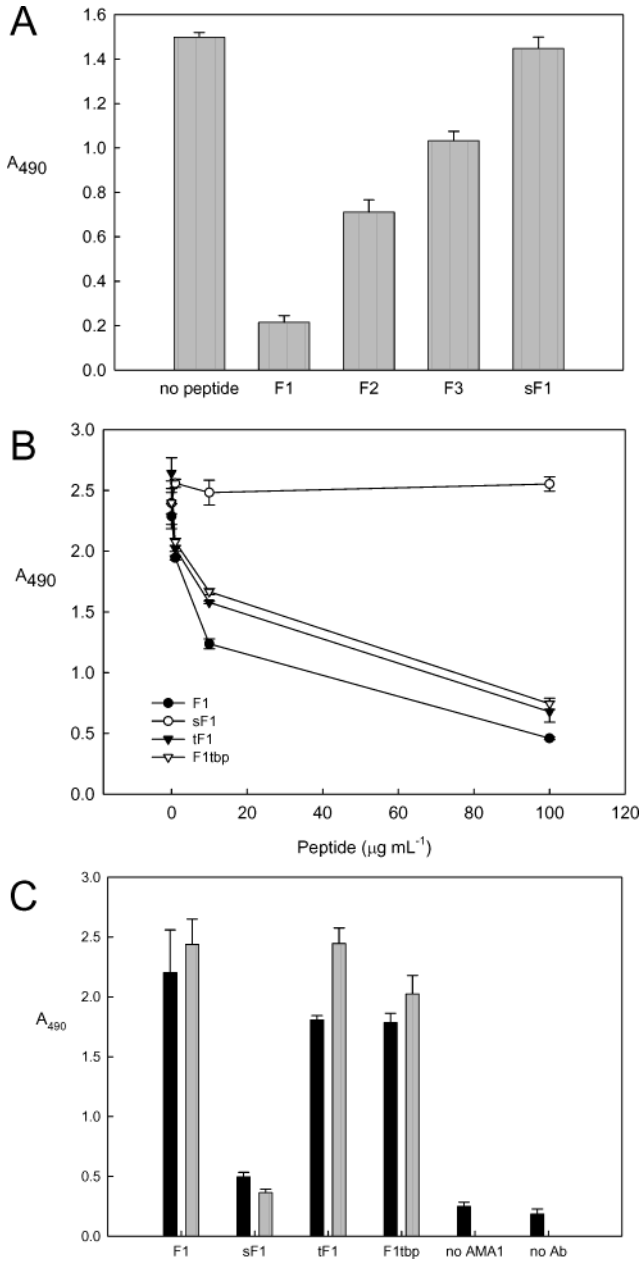

FIGURE 2: Peptide binding to *P. falciparum* AMA1. (A) Peptides F1−F3 and sF1 were competed against phage displaying F1 for binding to *P. falciparum* AMA1 strain 3D7. Phage binding to *P. falciparum* AMA1 was detected using an ELISA-based assay. (B) Competition assay for binding to phage displaying F1 using increasing amounts of peptides F1, tF1, F1tbp, and sF1 detected using an ELISA-based assay. (C) The F1 series peptides were bound to a plate, and their ability to capture *P. falciparum* AMA1 was assessed by an ELISA-based assay. AMA1 was added at either 10 (black bars) or 100 μg/mL (gray bars).

binding activity of F1 are in the C-terminal segment. These peptides were not able to inhibit invasion by the HB3 parasite strain or bind to AMA1 from the HB3 strain of *P. falciparum*, suggesting that the binding site for F1 and tF1 occurs in a region of variability in the primary amino acid sequence, 27 residues of which differ between the 3D7 and HB3 forms of *P. falciparum* AMA1. Peptide F1tbp was also tested against strain 3D7 and found to be equipotent with F1 in inhibiting invasion (IC_{50} = 10 μM; data not shown).

NMR Spectroscopy. ^{1}H NMR spectra of all peptides were characterized by a limited chemical shift dispersion that is not unusual for peptides of this size. Each peptide contained

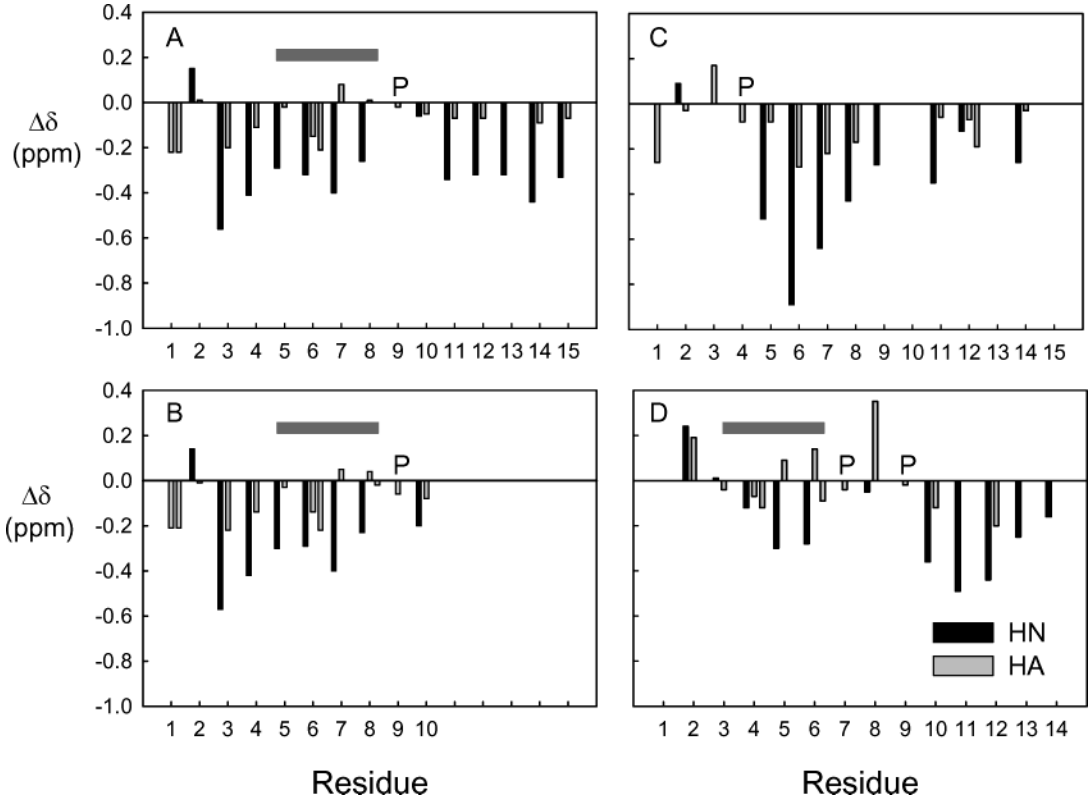

FIGURE 3: Deviation of chemical shifts from random coil values. Chemical shifts of backbone amide and $C^{\alpha}H$ resonances from (A) F1, (B) tF1, (C) sF1, and (D) F1tbp were compared to random coil chemical shift values published by Merutka *et al*. (*61*). The letter P indicates the presence of a proline residue, while the gray bar denotes the residues involved in type I β-turns. Two values are indicated for $C^{\alpha}H$ of each Gly residue.

at least one proline, with F1tbp containing two (Figure 1), and all of these prolines were observed to undergo cis−trans isomerization (not shown). For each peptide, the trans conformation dominated in solution, constituting approximately 95% of the total. While chemical shifts were assigned for some cis conformations, the structures described below are for the major trans conformers. ^{1}H chemical shifts were assigned for each of the peptides in the F1 family and F2 (see the Supporting Information). In addition, ^{13}C chemical shifts were assigned for peptide tF1. Chemical shifts for each of the peptides F1, tF1, F1s, and F1tbp in water have been deposited in the BioMagResBank (*34*). Translational diffusion coefficients were measured for F1 (1.24×10^{-10} m^2/s) and sF1 (1.39×10^{-10} m^2/s). Allowing for temperature and viscosity effects, these diffusion coefficients are similar to those of the peptides studied by Yao *et al*. (*32*), implying that F1 and sF1 are monomeric under the solution conditions used in this study.

Resonance assignments were made for all backbone and most side chain protons in peptides F1, tF1, and F1tbp in the major (trans) conformations. Assignments are missing because of spectral overlap for Ser8 ($C^{\alpha}H$ and $C^{\beta}H$), Gly10 (all), Ser13 (all), Gly15 (all), and the side chains of Leu9 ($C^{\gamma}H$ and $C^{\delta}H_3$) and Leu14 ($C^{\gamma}H$ and $C^{\delta}H_3$) in sF1, and for Arg2, Leu3, and Leu9 in F2. Deviations of amide and α proton chemical shifts from random coil values followed the same pattern for F1 and tF1 peptides except for the amide proton of Ala10, located at the truncation site in tF1 (Figure 3). This indicates that the backbone atoms in these two peptides are in similar environments and are thus likely to adopt similar conformations in solution.

Families of structures for each of the peptides were calculated using distance restraints obtained from two-dimensional homonuclear NOESY spectra. A summary of the medium-range, sequential, and intraresidue NOEs and dihedral restraints used in the final calculations in both DYANA and CNS is shown in Table 1. There were no long-range NOEs ($i - j > 4$), and no slowly exchanging protons were observed in amide exchange experiments (not shown). The final families of 20 structures for each peptide in the F1 series are shown in Figure 4, and a comparison of structural statistics is in Table 1. No distance violations of >0.2 Å or dihedral violations of >5° were observed in the final structures.

A well-defined conformation was not obtained for the F2 peptide, with an rmsd for the backbone in excess of 2.0 Å (structures not shown). This was partly attributable to missing chemical shift assignments as a result of spectral overlap, particularly for Arg2, Leu3, and Leu9. However, the chemical shifts that were assigned were close to random coil values (not shown), and only intraresidue and sequential NOE correlations were observed, implying that this peptide was flexible in solution and did not adopt a stable conformation.

The angular order parameter S is used to assess the precision of torsion angles within an ensemble of structures, with a value of 1 if the angle is identical over the family of structures and 0 if the angle is undefined. The S values for the ϕ and ψ angles of these peptides are presented in Figure S2 of the Supporting Information and those for the side chain χ^1 angles in Figure S3. For F1 and tF1, the ϕ and ψ angles were generally well-ordered ($S_{\phi,\psi} > 0.8$) over residues 2−9. F1 had lower S values for Ser11 and 12 ψ angles resulting

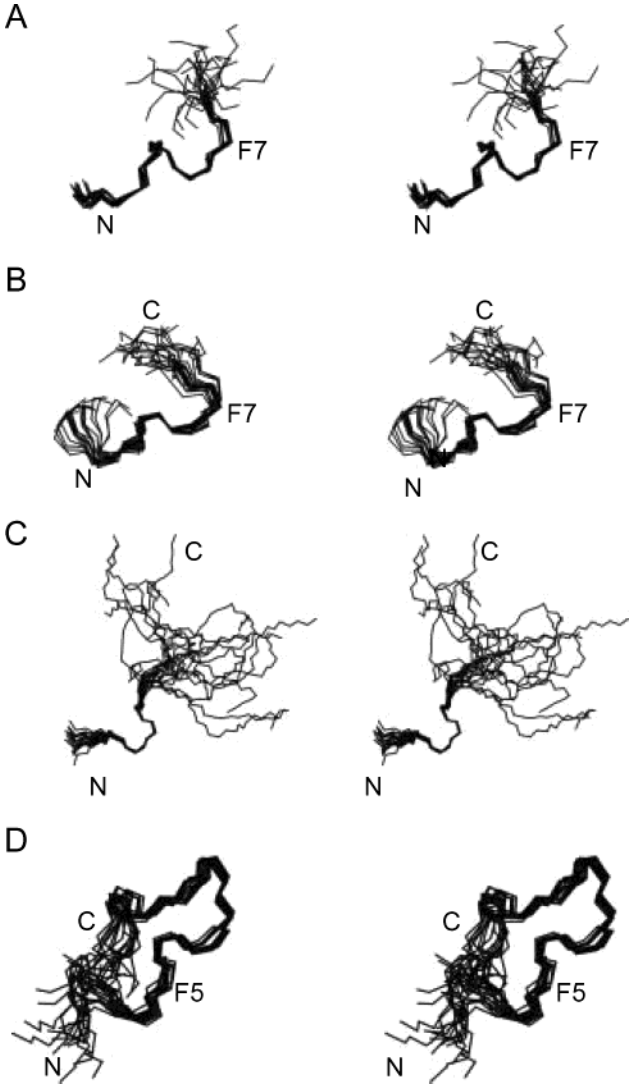

FIGURE 4: Structures of the F1 series of peptides. Superpositions of families of the 20 lowest-energy structures for (A) F1, (B) tF1, (C) sF1, and (D) F1tbp. Structures were superimposed over the backbone heavy atoms (N, C^{α}, and C) of residues 2−9 for F1 and tF1, residues 2−7 for sF1, and residues 2−13 for F1tbp. For F1, the poorly defined C-terminal region from residue 11 to 15 is not shown to facilitate comparison with the tF1 peptide. In the case of sF1, the poorly defined region (residues 8−14, where $S_{\phi,\psi} < 0.8$ for consecutive residues) is included to illustrate the lack of order over the LGFG sequence. For reference, the position of the equivalent Phe in F1, tF1, and F1tbp is labeled.

in disorder in the C-terminal tail in the family of structures. F1tbp was well-defined except for the first and last residues, while sF1 was poorly defined from residue 8 to the C-terminus, most likely reflecting the lack of resonance assignments and NOE restraints for these residues. Generally, the decrease in *S* values was reflected in the greater disorder observed in the family of structures (Figures 4, S2, and S3). Notably, the ϕ angle of Gly8 in F1 and tF1 and Gly6 of F1tbp showed a reduced *S* value. For residues with an *S* value of >0.8, the Karplus equation was used to back-calculate the expected $^3J_{HNH\alpha}$ value from the average ϕ angle. For F1, tF1, and F1tbp, none of these calculated coupling constants was below 6 Hz, in good agreement with the experimental data (Supporting Information). Residues occupying positions where small coupling constants (<5 Hz) would be expected were found to be glycines and prolines. *S* values for the F2

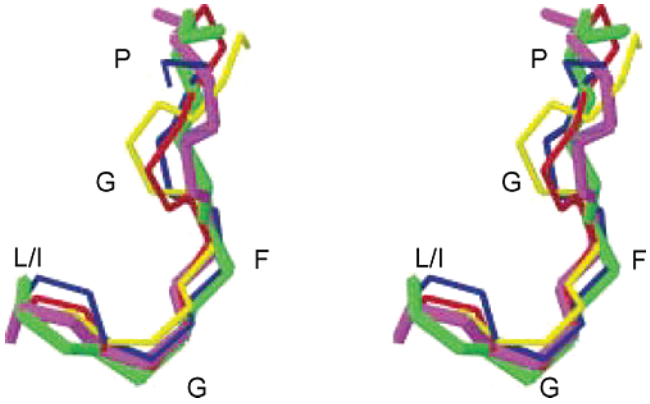

FIGURE 5: Overlay of the F1 peptide with the truncated peptide (tF1) and the cyclized peptide (F1tbp). The closest-to-average structures for each of peptides F1 (red), tF1 (blue), and F1tbp (yellow) are superimposed over the backbone atoms of residues which are critical for biological activity (Leu5−Pro9 for F1 and tF1 and Ile3−Pro7 for F1tbp). The rmsd for the backbone heavy atoms (N, C^{α}, and C) for these peptides was 0.75 Å. Also superimposed are the LGFGP motif from crystal structures of a triacylglycerol hydrolase from *G. candidum* (green) and the L3 subunit of the 50S ribosome from *H. marismortui* (magenta), which were obtained from the Protein Data Bank. In addition to these two proteins, the LGFGP sequence occurs in approximately 120 other proteins that have been sequenced, but to date, no other structures have been determined experimentally.

peptide were generally <0.6 (not shown), with residues scattered in all regions of the Ramachandran plot, confirming that this peptide does not adopt a dominant, ordered conformation in solution.

The F1 peptide had an ordered backbone over residues Trp2−Pro9, but the N-terminus and the five C-terminal residues were disordered (Figure 4A). The backbone ϕ and ψ angles for residues Gly6 and Phe7 indicate the presence of a type I β-turn between Leu5 and Gly8 in this peptide. The truncated version of this peptide, tF1, also had an ordered backbone over residues Trp2−Pro9 (Figure 4B) that could be superimposed over the equivalent residues in F1 with an rmsd of 0.76 Å over the backbone heavy atoms (Figure 5). This was consistent with the chemical shift data in Figure 3, which suggested that the protons in the two peptides experienced the same chemical environments. The inactive control peptide sF1 contained a type III β-turn encompassing Ser3−Phe6 (Figure 4C). However, it was not possible to overlay this peptide onto any of the other peptides in the F1 series. Notably, the LGFG motif involved in a β-turn in F1 and tF1 was not involved in a turn structure in the sF1 peptide. F1tbp was well-defined over the backbone atoms for residues Ile3−Phe11 (Figures 4D and 5), and contained a type I β-turn at residues Ile3−Gly6.

Peptides in aqueous solution often sample a range of conformations in the absence of any structural restraints such as disulfide or lactam bridges. The finding that F1 and tF1 adopted a type I β-turn at residues Leu3−Gly6 is unexpected, but presumably reflects the strong propensity of this sequence to form such a turn (as discussed below). The presence of a type I β-turn at residues Ile3−Gly6 of F1tbp is less surprising because the termini of this peptide are linked by a disulfide. The similarities in the patterns of deviations from random coil chemical shifts for the NH and $C^{\alpha}H$ resonances from these regions of F1, tF1, and F1tbp (Figure 3), however, support the contention that they do adopt similar conforma-

tions in solution. The deviations of the NH shifts for Ile3 and Gly4 of F1tbp differ slightly from those for F1 and tF1, being closer to random coil, but the corresponding $C^{\alpha}H$ $\Delta\delta$ values are in good agreement. Wishart *et al*. (*44*) noted that the positions of β-turns in proteins could often be distinguished by pairs of $C^{\alpha}H$ $\Delta\delta$ values with opposite signs (+ and −, or − and +). This is indeed the pattern displayed by the Gly and Phe residues that occupy positions $i + 1$ and $i + 2$ in the structures of F1, tF1, and F1tbp (Figure 3). On the other hand, when $\Delta\delta$ values for NH and $C^{\alpha}H$ resonances of type I β-turns in a range of small disulfide-stabilized polypeptides with well-defined structures are compared (Figure S4 of the Supporting Information) (*45*−*52*), it becomes clear that the patterns vary considerably, making it difficult to assess turn formation from such data alone.

DISCUSSION

In this study, we have examined the structural features of a series of peptides that bind to AMA1 and inhibit merozoite invasion of host red blood cells. The F1 and F2 families of peptides were identified, using phage-display techniques, as having the ability to bind specifically to *P. falciparum* AMA1 strain 3D7 and, in the case of F2, *P. chabaudi* AMA1 strain DS (the sequence of which is 52% identical with that of *P. falciparum* AMA1) as well. Once an alanine scan had identified the residues in F1, Leu5−Pro9, that were important for binding to *P. falciparum* AMA1 (*1*), a truncated 10-residue peptide (tF1) was designed that competed with F1 phage for binding to AMA1 and was as effective as F1 in binding to AMA1 and inhibiting merozoite invasion of red blood cells (Figures 2 and S1). F1 and tF1 exhibited similar inhibitory profiles, blocking merozoites of the *P. falciparum* 3D7 strain but not those of the *P. falciparum* HB3 strain (Figure S1). In addition, the monoclonal antibody, mAb4G2, which binds to *P. falciparum* AMA1 and can inhibit the invasion of red blood cells by the parasite (*53*), blocks the binding of F1, but not F2 or F3, to *P. falciparum* AMA1 (*1*). These results suggest that the F1 and F2 peptides bind to two different but overlapping sites on AMA1.

Another peptide, F1tbp, representing a disulfide-stabilized peptide fragment of the latent transforming growth factor-β binding protein with a sequence similar to that of F1, was also examined for affinity for *P. falciparum* AMA1. It was found to be as effective as tF1 in competing for *P. falciparum* AMA1 with phage displaying F1 (Figure 2) and equipotent with F1 in inhibiting the invasion of red blood cells by 3D7 merozoites (Figure S1). The sequence similarity and occurrence of common structural features in F1 and latent TGF-β binding protein raise the intriguing possibility that AMA1 could bind a latent TGF-β binding protein-like molecule on the surface of host red blood cells during merozoite invasion. Alternatively, the homology between F1 peptide and latent TGF-β binding protein may be coincidental and have no biological implications for invasion. Further work is required to distinguish between these two possibilities.

As these peptides exhibited interesting biological properties, their solution structures were determined. Each member of the F1 family contained an ordered backbone in the N-terminal region of the peptide, but F2 did not adopt a preferred conformation in solution. A lack of dispersion in the chemical shifts hindered the assignment of NOE cross-peaks for this peptide, but those chemical shifts that were assigned were close to random coil values, as would be expected for an unstructured peptide. This of course does not preclude this peptide from adopting a stable conformation upon binding to its target epitope.

Each of the peptides in the F1 family was found to contain a β-turn structure. In F1 and tF1, this β-turn encompasses residues which had been identified previously by alanine scanning as being important for both binding to AMA1 and the ability to inhibit invasion. This suggests that these turns may be involved in the binding interactions. Gly6 and Phe7, which are in the second and third positions, respectively, of the turns were the residues for which the largest decreases in binding activity were observed when they were replaced with alanine (*1*). These residues, which may be critical for binding or maintaining the turn structure, or possibly both, are shown mapped onto the F1 structure in Figure 6. It was noted by Skelton *et al*. (*23*) that in many peptides identified by phage-display techniques a cluster of two or three hydrophobic residues was critical for binding to target receptors. In the case of F1 and tF1 in our study, Leu5 and Phe7 may be fulfilling this role, as suggested by the alanine scan.

F1tbp contained a type I β-turn encompassing residues Ile3−Gly6 and, as shown in Figure 5, superimposed very well with the LGFGP motif of both F1 and tF1 (rmsd $\sim$ 0.65 Å), even though the flanking sequence was quite distinct from that of F1 and tF1 and the N- and C-termini of F1tbp were linked by a disulfide bond. The F1tbp sequence forms part of putative EGF-like calcium binding domain in the latent TGF-β binding protein (*42*). F1tbp corresponds to residues 527−540 of the full-length protein, that is, the last 14 of the 40 residues in the putative EGF-like calcium binding domain. There are currently no structures for the latent TGF-β binding protein that can be compared with the structure determined for F1tbp, but other human EGF domains have been found to contain a β-turn motif in this location, although the turn type varies. In human factor VII, it is a type I turn (*54*), as observed for F1tbp, while the corresponding region from human factor IX is a type II turn (*55*).

Two sets of protein structures containing the LGFGP motif have appeared recently in the Protein Data Bank (*56*). These include a triacylglycerol hydrolase from *Geotrichum candidum* [PDB entry 1THG (*56*, *57*)] and a series of structures of subunits of the 50S ribosome from *Haloarcula marismortui* complexed with several different antibiotics [PDB entries 1KA8, 1K9M, 1KD1, and 1KQS (*56*, *58*)]. The LGFGP motif from these structures and those determined for F1, tF1, and F1tbp overlay remarkably closely, with a pairwise backbone rmsd of 0.75 Å (Figure 5). This indicates that the L(I)GFGP sequence has a strong propensity to adopt a β-turn structure, largely independent of the surrounding sequence. This may be a consequence of the nonpolar character of the residues involved. Nonetheless, it must be acknowledged that the peptide structures described in our study represent the averages of ensembles of interconverting conformations which are likely to include conformations in which the turn structures are less well defined than indicated in Figure 4. The fact that NMR data sets for three peptides, one of which is stabilized by a disulfide bridge, define a type I β-turn in homologous regions of their sequences, and

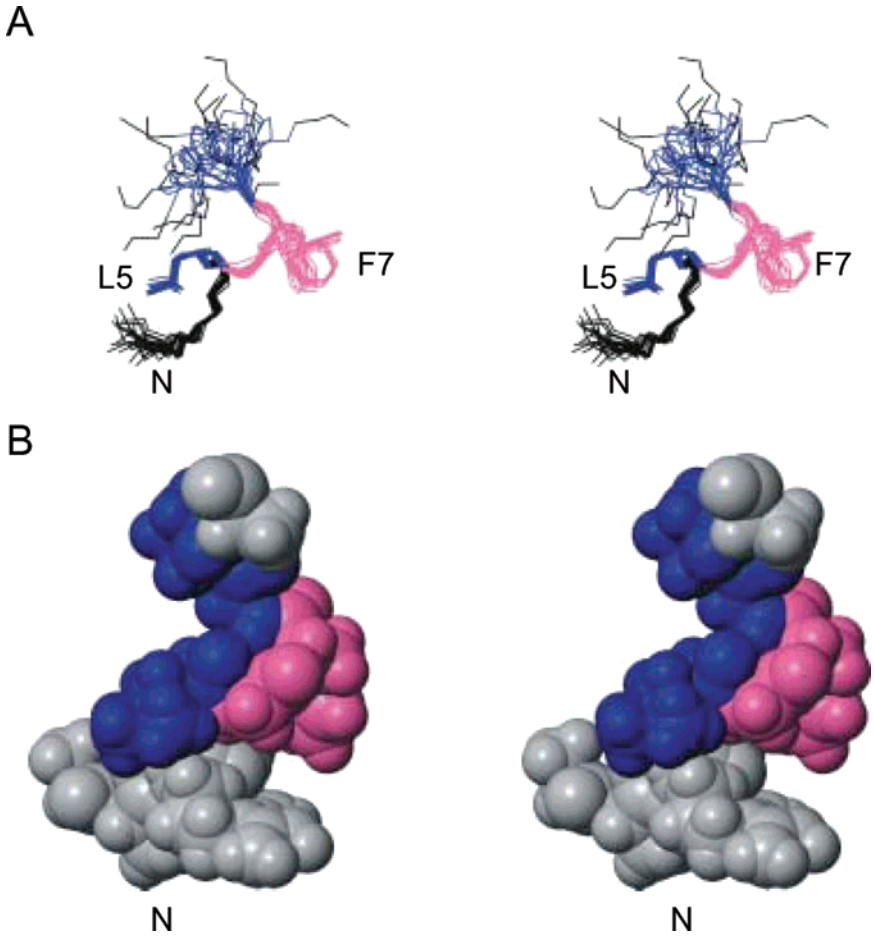

FIGURE 6: Biologically relevant residues in F1. (A) Family of F1 structures. Heavy atoms in the backbone (N, C^{α}, and C) for residues Gly1−Ala10 and the side chains of Leu5 and Phe7 are shown. The side chain of Leu5 is well-defined because of a significant number of NOEs to nearby residues (six intraresidue, seven sequential, and four medium-range, following elimination of NOEs that were redundant with the covalent geometry). Angular order parameters for all side chains of this and other peptides are summarized in the Supporting Information (Figure S3). (B) CPK surface representation of the closest-to-average structure over the family. Both are color-coded according to the results of the alanine scan; when replaced with alanine, residues in gray had no effect, those in blue a moderate effect, and those in pink large effects on the ability of F1 to bind AMA1.

that the homologous sequence in larger proteins adopts an identical structure, implies that this local structural element is relatively stable. We therefore believe it is unlikely that their conformations will change significantly upon binding to AMA1, given the conservation of the structure observed for this motif across several unrelated peptides and proteins, but this needs to be established experimentally.

The control peptide, sF1, had no recognizable structural motif over the residues where a turn was observed in the F1 and tF1 peptides, instead containing a type III β-turn near the N-terminal. This is likely to be due at least in part to the presence of a serine rather than a proline at the end of the LGFGP motif that is required for biological activity in F1.

β-Turns are now recognized as a common structural motif that is involved in the interactions of peptides and proteins with their target receptors, and there is growing interest in the development of nonpeptide, drug-like molecules that mimic these structures (*59*). A recent example is an opiate analogue that mimics type I β-turns in enkephalin (*60*). The molecule has a rigid, bicyclic structure with four sites of diversity, including the i to $i + 3$ positions of the corresponding β-turn. Importantly, this molecule can be readily synthesized using commercial solid-state techniques. Our finding that a common β-turn structure in F1 and tF1 encompasses the residues essential for binding to AMA1, and that F1tbp shares this structural feature, suggests that it should be possible to develop nonpeptide mimetics of the key elements of these inhibitory peptides. These have the potential to bind AMA1 and block its interactions with the erythrocyte membrane, and thus to block merozoite invasion at the clinically important stage of the disease.

ACKNOWLEDGMENT

We are grateful to Mark Hinds, Shenggen Yao, and Kevin Barnham for valuable discussions.

SUPPORTING INFORMATION AVAILABLE

Five tables of chemical shifts and four figures. This material is available free of charge via the Internet at http://pubs.acs.org.

REFERENCES

1. Li, F., Dluzewski, A. R., Coley, A. M., Thomas, A. W., Tilley, L., Anders, R. F., and Foley, M. (2002) *J. Biol. Chem. 277*, 50303−50310.
2. Peterson, M. G., Marshall, V. M., Smythe, J. A., Crewther, P. E., Lew, A., Silva, A., Anders, R. F., and Kemp, D. J. (1989) *Mol. Cell. Biol. 9*, 3151−3154.

3. Peterson, M. G., Nguyen-Dinh, P., Marshall, V. M., Elliott, J. F., Collins, W. E., Anders, R. F., and Kemp, D. J. (1990) *Mol. Biochem. Parasitol. 39*, 279−283.
4. Thomas, A. W., Bannister, L. H., and Waters, A. P. (1990) *Parasite Immunol. 12*, 105−113.
5. Waters, A. P., Thomas, A. W., Deans, J. A., Mitchell, G. H., Hudson, D. E., Miller, L. H., McCutchan, T. F., and Cohen, S. (1990) *J. Biol. Chem. 265*, 17974−17979.
6. Chitnis, C. E., and Blackman, M. J. (2000) *Parasitol. Today 16*, 411−415.
7. Deans, J. A., Knight, A. M., Jean, W. C., Waters, A. P., Cohen, S., and Mitchell, G. H. (1988) *Parasite Immunol. 10*, 535−552.
8. Collins, W. E., Pye, D., Crewther, P. E., Vandenberg, K. L., Galland, G. G., Sulzer, A. J., Kemp, D. J., Edwards, S. J., Coppel, R. L., and Sullivan, J. S. (1994) *Am. J. Trop. Med. Hyg. 51*, 711−719.
9. Crewther, P. E., Matthew, M. L., Flegg, R. H., and Anders, R. F. (1996) *Infect. Immun. 64*, 3310−3317.
10. Anders, R. F., Crewther, P. E., Edwards, S., Margetts, M., Matthew, M. L., Pollock, B., and Pye, D. (1998) *Vaccine 16*, 240−247.
11. Deans, J. A., Alderson, T., Thomas, A. W., Mitchell, G. H., Lennox, E. S., and Cohen, S. (1982) *Clin. Exp. Immunol. 49*, 297−309.
12. Thomas, A. W., Deans, J. A., Mitchell, G. H., Alderson, T., and Cohen, S. (1984) *Mol. Biochem. Parasitol. 13*, 187−199.
13. Kocken, C. H., Hundt, E., Knapp, B., Brazel, D., Enders, B., Narum, D. L., Wubben, J. A., and Thomas, A. W. (1998) *Infect. Immun. 66*, 373−375.
14. Narum, D. L., Ogun, S. A., Thomas, A. W., and Holder, A. A. (2000) *Infect. Immun. 68*, 2899−2906.
15. Triglia, T., Healer, J., Caruana, S. R., Hodder, A. N., Anders, R. F., Crabb, B. S., and Cowman, A. F. (2000) *Mol. Microbiol. 38*, 706−718.
16. Hehl, A. B., Lekutis, C., Grigg, M. E., Bradley, P. J., Dubremetz, J. F., Ortega-Barria, E., and Boothroyd, J. C. (2000) *Infect. Immun. 68*, 7078−7086.
17. Donahue, C. G., Carruthers, V. B., Gilk, S. D., and Ward, G. E. (2000) *Mol. Biochem. Parasitol. 111*, 15−30.
18. Pasqualini, R., and Ruoslahti, E. (1996) *Mol. Psychiatry 1*, 423.
19. Jost, P. J., Harbottle, R. P., Knight, A., Miller, A. D., Coutelle, C., and Schneider, H. (2001) *FEBS Lett. 489*, 263−269.
20. Isalan, M., Patel, S. D., Balasubramanian, S., and Choo, Y. (2001) *Biochemistry 40*, 830−836.
21. Lesinski, G. B., Smithson, S. L., Srivastava, N., Chen, D., Widera, G., and Westerink, M. A. (2001) *Vaccine 19*, 1717−1726.
22. McConnell, S. J., Kendall, M. L., Reilly, T. M., and Hoess, R. H. (1994) *Gene 151*, 115−118.
23. Skelton, N. J., Chen, Y. M., Dubree, N., Quan, C., Jackson, D. Y., Cochran, A., Zobel, K., Deshayes, K., Baca, M., Pisabarro, M. T., and Lowman, H. B. (2001) *Biochemistry 40*, 8487−8498.
24. Lowman, H. B., Chen, Y. M., Skelton, N. J., Mortensen, D. L., Tomlinson, E. E., Sadick, M. D., Robinson, I. C., and Clark, R. G. (1998) *Biochemistry 37*, 8870−8878.
25. Fairbrother, W. J., Christinger, H. W., Cochran, A. G., Fuh, G., Keenan, C. J., Quan, C., Shriver, S. K., Tom, J. Y., Wells, J. A., and Cunningham, B. C. (1998) *Biochemistry 37*, 17754−17764.
26. Trager, W., and Jensen, J. B. (1976) *Science 193*, 673−675.
27. Dluzewski, A. R., Ling, I. T., Rangachari, K., Bates, P. A., and Wilson, R. J. M. (1984) *Trans. R. Soc. Trop. Med. Hyg. 78*, 622−624.
28. Bax, A., Griffey, R. H., and Hawkins, B. L. (1983) *J. Magn. Reson. 55*, 301−315.
29. Muller, L. (1979) *J. Am. Chem. Soc. 101*, 4481−4484.
30. Gibbs, S. J., and Johnson, C. S. (1991) *J. Magn. Reson. 93*, 395−402.
31. Dingley, A. J., Mackay, J. P., Chapman, B. E., Morris, M. B., Kuchel, P. W., Hambly, B. D., and King, G. F. (1995) *J. Biomol. NMR 6*, 321−328.
32. Yao, S., Howlett, G. J., and Norton, R. S. (2000) *J. Biomol. NMR 16*, 109−119.
33. Bartels, C., Xia, T. H., Billeter, M., Güntert, P., and Wüthrich, K. (1995) *J. Biomol. NMR 6*, 1−10.
34. Seavey, B. R., Farr, E. A., Westler, W. M., and Markley, J. L. (1991) *J. Biomol. NMR 1*, 217−236.
35. Baxter, N. J., and Williamson, M. P. (1997) *J. Biomol. NMR 9*, 359−369.
36. Güntert, P., Mumenthaler, C., and Wüthrich, K. (1997) *J. Mol. Biol. 273*, 283−298.
37. Brünger, A. T., Adams, P. D., Clore, G. M., DeLano, W. L., Gros, P., Grosse-Kunstleve, R. W., Jiang, J. S., Kuszewski, J., Nilges, M., Pannu, N. S., Read, R. J., Rice, L. M., Simonson, T., and Warren, G. L. (1998) *Acta Crystallogr. D54*, 905−921.
38. Linge, J. P., and Nilges, M. (1999) *J. Biomol. NMR 13*, 51−59.
39. Laskowski, R. A., Rullmannn, J. A., MacArthur, M. W., Kaptein, R., and Thornton, J. M. (1996) *J. Biomol. NMR 8*, 477−486.
40. Koradi, R., Billeter, M., and Wüthrich, K. (1996) *J. Mol. Graphics 14*, 51−55.
41. Altschul, S. F., Madden, T. L., Schaffer, A. A., Zhang, J., Zhang, Z., Miller, W., and Lipman, D. J. (1997) *Nucleic Acids Res. 25*, 3389−3402.
42. Kanzaki, T., Olofsson, A., Moren, A., Wernstedt, C., Hellman, U., Miyazono, K., Claesson-Welsh, L., and Heldin, C. H. (1990) *Cell 61*, 1051−1061.
43. Oklu, R., and Hesketh, R. (2000) *Biochem. J. 352*, 601−610.
44. Wishart, D. S., Sykes, B. D., and Richards, F. M. (1992) *Biochemistry 31*, 1647−1651.
45. Hansen, P. E., Kem, W. R., Bieber, A. L., and Norton, R. S. (1992) *Eur. J. Biochem. 210*, 231−240.
46. Norton, R. S., Cross, K., Braach-Maksvytis, V., and Wachter, E. (1993) *Biochem. J. 293*, 545−551.
47. Pallaghy, P. K., Duggan, B. M., Pennington, M. W., and Norton, R. S. (1993) *J. Mol. Biol. 234*, 405−420.
48. Manoleras, N., and Norton, R. S. (1994) *Biochemistry 33*, 11051−11061.
49. Tudor, J. E., Pallaghy, P. K., Pennington, M. W., and Norton, R. S. (1996) *Nat. Struct. Biol. 3*, 317−320.
50. Tudor, J. E., Pennington, M. W., and Norton, R. S. (1998) *Eur. J. Biochem. 251*, 133−141.
51. Barnham, K. J., Dyke, T. R., Kem, W. R., and Norton, R. S. (1997) *J. Mol. Biol. 268*, 886−902.
52. Hill, J. M., Alewood, P. F., and Craik, D. J. (1996) *Biochemistry 35*, 8824−8835.
53. Kocken, C. H., van der Wel, A. M., Dubbeld, M. A., Narum, D. L., van de Rijke, F. M., van Gemert, G. J., van der Linde, X., Bannister, L. H., Janse, C., Waters, A. P., and Thomas, A. W. (1998) *J. Biol. Chem. 273*, 15119−15124.
54. Muranyi, A., Finn, B. E., Gippert, G. P., Forsen, S., Stenflo, J., and Drakenberg, T. (1998) *Biochemistry 37*, 10605−10615.
55. Baron, M., Norman, D. G., Harvey, T. S., Handford, P. A., Mayhew, M., Tse, A. G., Brownlee, G. G., and Campbell, I. D. (1992) *Protein Sci. 1*, 81−90.
56. Berman, H. M., Westbrook, J., Feng, Z., Gilliland, G., Bhat, T. N., Weissig, H., Shindyalov, I. N., and Bourne, P. E. (2000) *Nucleic Acids Res. 28*, 235−242.
57. Schrag, J. D., and Cygler, M. (1993) *J. Mol. Biol. 230*, 575−591.
58. Hansen, J. L., Ippolito, J. A., Ban, N., Nissen, P., Moore, P. B., and Steitz, T. A. (2002) *Mol. Cell 10*, 117−128.
59. Golebiowski, A., Klopfenstein, S. R., and Portlock, D. E. (2001) *Curr. Opin. Drug Discovery Dev. 4*, 428−434.
60. Eguchi, M., Shen, R. Y., Shea, J. P., Lee, M. S., and Kahn, M. (2002) *J. Med. Chem. 45*, 1395−1398.
61. Merutka, G., Dyson, H. J., and Wright, P. E. (1995) *J. Biomol. NMR 5*, 14−24.

BI034376B